JOC The Journal of Organic Chemistry

Article

pubs.acs.org/joc

On the Absolute Configuration of Chiral 1,4-Dihydropyridazines Synthesized by Organocatalysed Reactions

Na Lin,[†,‡] Cristina Forzato,[§] Federico Berti,[§] Fulvia Felluga,[§] Patrizia Nitti,[§] Giuliana Pitacco,[§] and Sonia Coriani*[,§]

[†]State Key Laboratory of Crystal Materials, Shandong University, 250100 Jinan, Shandong, P. R. China

[‡]Centre for Theoretical and Computational Chemistry, University of Tromsø, N-9037 Tromsø, Norway

[§]Dipartimento di Scienze Chimiche e Farmaceutiche, Università degli Studi di Trieste, 34127 Trieste, Italy

Supporting Information

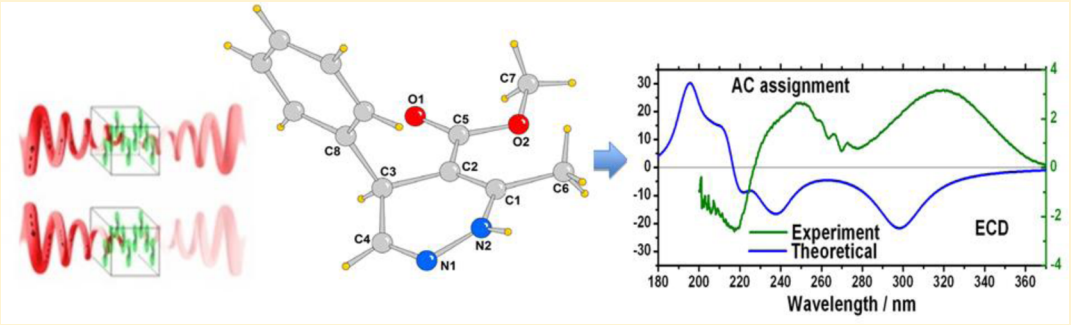

ABSTRACT: A computational investigation of the specific optical rotation and of the electronic circular dichroism spectra of two chiral 1,4-dihydropyridazines was performed and compared with existing experimental data to verify a previous assignment of their absolute configuration based on a well-accepted mechanism of catalysis of the organocatalyst used in their synthesis. Both the optical rotation and circular dichroism calculations indicate that the absolute configuration is opposite to the one assigned on the basis of the mechanism originally assumed. An alternative reaction mechanism is therefore suggested.

INTRODUCTION

1,4-Dihydropyridazines are a class of compounds that is receiving significant attention for their potential use as antihypertensive and vasodilating agents[1] because they are very similar to 1,4-dihydropyridines, which have shown such biological activities.[2] Moreover, in 1994, Chiou reported that fused 1,4-dihydropyridazines showed ocular anti-inflammatory activity as an interleukin-1 blocker.[3]

Although there is an increasing number of papers and patents regarding the synthesis of the pyridazine ring, not many syntheses are present in the literature for the 1,4-dihydro derivatives. Very often, these compounds are obtained only as intermediates in the synthesis of pyridazines,[4] pyrrols,[5] or phthalazines.[6]

Among all of the methods proposed so far to synthesize 1,4-dihydropyridazines,[7−11] only two are concerned with optically active species. The first one was reported in 2008 by Buonora et al., who synthesized four chiral 6-phenyl-4,4-disubstituted-1,4-dihydropyridazines by reaction of chiral α,α-disubstituted 1,4-diketones with hydrazine. The 4,5-dihydropyridazines formed in this way spontaneously tautomerized into the 1,4-dihydropyridazines.[12]

In the second asymmetric synthesis,[13] proposed by some of us in 2010, chiral nonracemic 1,4-dihydropyridazines (Figure 1) were obtained by reaction of 1,2-diaza-1,3-dienes with arylacetaldehydes under organocatalytic conditions. Their enantiomeric excesses ranged from 25 to 78%. The absolute configuration of the newly formed compounds was tentatively assigned as (*S*) on the basis of the well-accepted catalysis mechanism of L-proline[14] used as the organocatalyst, namely, a preferential *re*−*si* facial attack of the enamine intermediate, formed in situ from the aldehyde and proline (or protonated

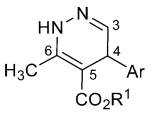

R^1 = Et; Ar = C_6H_5-: (+)-**1**
R^1 = Me; Ar = C_6H_5-: (+)-**2**
R^1 = Me; Ar = *p*-Br-C_6H_4-: (+)-**3**
R^1 = Me; Ar = *p*-EtO-C_6H_4-: (+)-**4**
R^1 = Me; Ar = *p*-NO_2-C_6H_4-: (+)-**5**
R^1 = Me; Ar = *o*-NO_2-C_6H_4-: (+)-**6**
R^1 = Me; Ar = *m*-NO_2-C_6H_4-: (+)-**7**

Figure 1. The chiral 1,4-dihydropyridazines (+)-**1** to (+)-7 synthesized in our previous work.[13]

Received: June 24, 2013
Published: November 4, 2013

(*S*)-(+)-1-(2-pyrrolidinylmethyl)pyrrolidine, 2PMP), onto the electrophile (vide infra).

Since the 1,4-dihydropyridazines synthesized in our previous work showed a very high value of specific optical rotation, we decided to carry out a computational investigation of the optical rotation power (OR) of two selected 1,4-dihydropyridazines to verify our previous assignment and hereby also evaluate the reliability of the empirical rules used. Electronic circular dichroism (ECD) spectra were calculated as well and compared to the experimentally spectra to confirm further the correctness of the assignment.

The two 1,4-dihydropyridazines chosen for the computational study are methyl 6-methyl-4-phenyl-1,4-dihydropyridazine-5-carboxylate [labeled (+)-**2** in Figure 1] and methyl 4-(4-bromophenyl)-6-methyl-1,4-dihydropyridazine-5-carboxylate [labeled (+)-**3** in Figure 1]. It is reasonable to assume that, because of the same synthetic procedure being adopted, all chiral 1,4-dihydropyridazines in Figure 1 have the same absolute configuration. Compound **2** was selected because it is the smallest of the 1,4-dihydropyridazines originally synthesized and therefore the less demanding from a computational point of view. Compound **3** was chosen mainly because it is potentially well-suited for an X-ray investigation of its absolute configuration, if it is crystallized in sufficient amounts.

The details of our calculations are given in the Results section followed by a discussion of the results and the conclusions of our study.

RESULTS

Computational Methodology. As the two selected 1,4-dihydropyridazines can be expected to possess some degree of conformational flexibility, we began our investigation with a conformational search to identify their most stable conformers. Starting from the trial model structure of the 1,4-dihydropyridazine **2** in (*S*) configuration, shown in Figure 2, the search

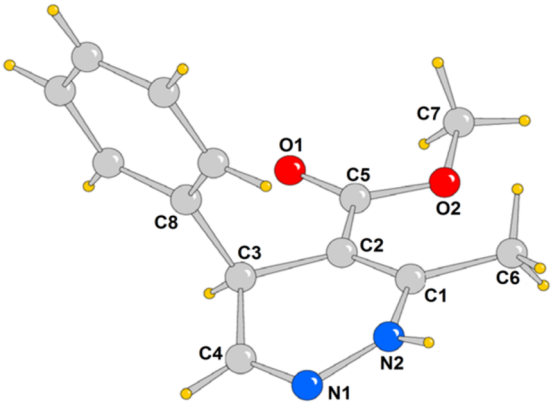

Figure 2. The model structure of (*S*)-**2**.

was performed by rotating both the phenyl group and the carbomethoxy group every 45 degrees around the C3−C8 and C2−C5 bonds, respectively, and by bending both the dihydropyridazinic ring and NH group 30 degrees up and down with respect to its medium plane. This generated 360 different potential conformers. Each structure was subsequently optimized in the gas phase at the density functional theory (DFT) level using the hybrid Becke three parameters Lee−Yang−Parr (B3LYP) functional[15] and the 6-31G(d) basis set. By inspecting the final energies, it was found that the optimizations ended up into four different structures, which were then reoptimized at the B3LYP level in the larger aug-cc-pVDZ basis set, both in the gas phase and in solution. For the calculations in solution, the polarizable continuum model (PCM)[16] was applied, where the cavities were defined by placing a sphere on all of the non-hydrogen elements, with default values of the radii. Methanol (CH_3OH) and acetonitrile (CH_3CN) were chosen as solvents, with dielectric constants of 32.630 and 35.688, respectively.

The geometries finally evolved into two structures (here labeled **2-c1** and **2-c2**) both in the gas phase and in solution (Figure 3). For compound **3**, we generated the starting

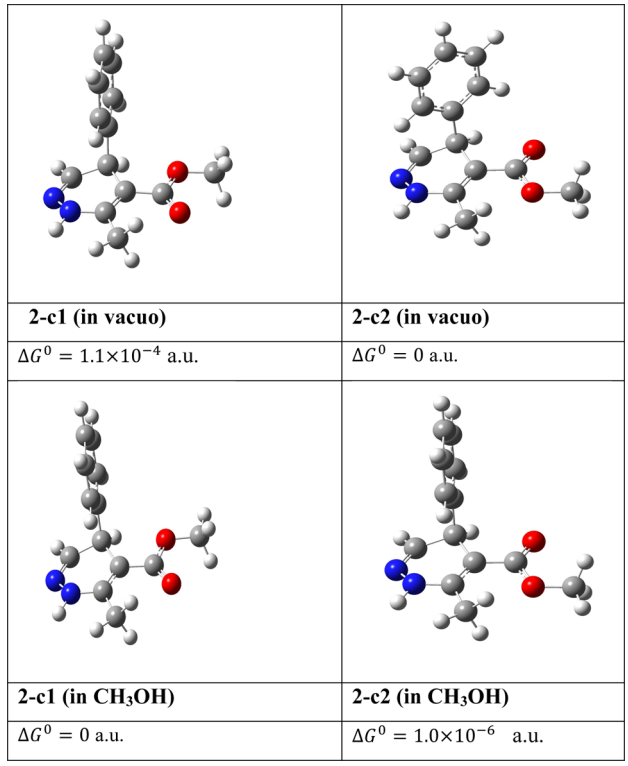

Figure 3. Compound **2**. Optimized geometries of the **c1** and **c2** conformers, both in the gas phase and in methanol, at the B3LYP/aug-cc-pVDZ level of theory.

structures from the (*S*)-**2** conformers by introducing the Br atom on the phenyl ring in para position and reoptimizing at the B3LYP/aug-cc-pVDZ level. This also yielded two stable conformers, labeled **3-c1** and **3-c2**, which are shown in Figure 4. We confirmed that all optimized structures corresponded to true energy minima by computing their fundamental vibrational frequencies. All geometry optimizations as well as the necessary calculations of the vibrational normal modes of the electronic ground state were carried out using the Gaussian 03 program suite.[17]

Once the stable conformers of the two compounds were identified, ECD and OR calculations in the gas phase and in the two above-mentioned solvents were performed on each of them using the B3LYP functional as well as its Coulomb-attenuated variant, CAM-B3LYP,[18] in its standard parametrization (α = 0.190, β = 0.460, and μ = 0.330) along with the aug-cc-pVDZ basis set. One-photon absorption (OPA) spectra were also obtained as a side product of our ECD

dx.doi.org/10.1021/jo401343y | J. Org. Chem. 2013, 78, 11670−11679

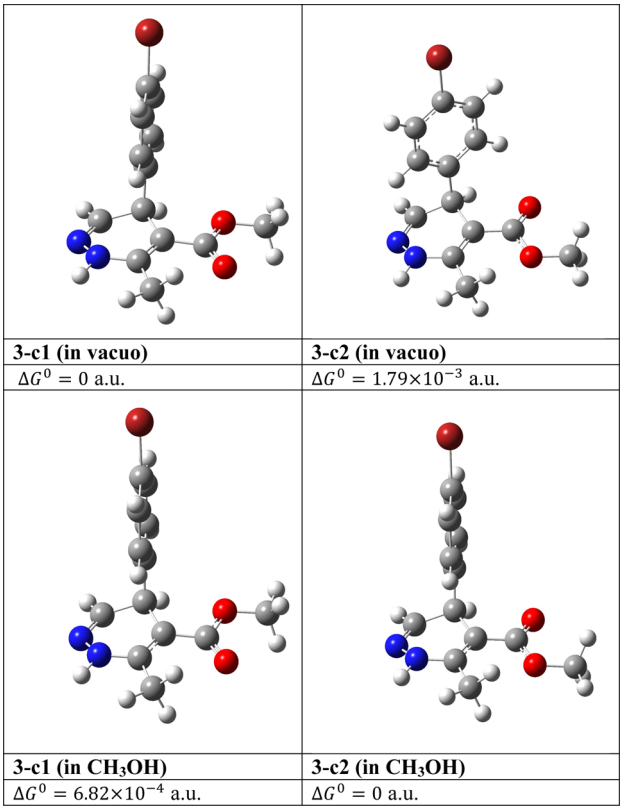

Figure 4. Compound **3**. Optimized geometries of the **c1** and **c2** conformers, both in the gas phase and in methanol, at the B3LYP/aug-cc-pVDZ level of theory.

calculations. The DALTON program suite[19] was employed for the property calculations, and London orbitals were adopted to remove gauge-origin dependencies. We refer to the Supporting Information as well as to ref 20 (and references therein) for additional information on the theoretical background and methodological procedure adopted in such calculations. Note that the OPA and ECD spectra of each conformer were generated from calculated molecular parameters (specifically, oscillator and rotational strengths) of the 15 lowest electronic excited states of each chemical species by convolution with a Lorentzian line shape function with a broadening lifetime value (fwhm) of 0.2 eV (chosen to show the best agreement with the experimental profiles).

Finally, the total optical rotation, and the ECD and OPA spectra of each selected 1,4-dihydropyridazines were generated by Boltzmann's average of the computed quantities of each conformer according to

$$P^{\mathrm{avg}}(\omega) = \sum_{i=c1,c2} P_i(\omega) X_i \tag{1}$$

where $P_i(\omega)$ indicates the given property of conformer i and X_i is its Boltzmann population fraction

$$X_i = \frac{\exp \frac{-\Delta G_i^0}{kT}}{\sum_{i=c1,c2} \exp \frac{-\Delta G_i^0}{kT}} \tag{2}$$

where k is the Boltzmann constant, T is the temperature in Kelvin, and $\Delta G_i^0 = (G_i^0 - G_0^0)$ is the Gibbs free energy change (at 298.15 K and 1 atm) of conformer i with respect to the Gibbs free energy, G_0^0, of the lowest-lying conformer. The Gibbs free energies calculated at the B3LYP/aug-cc-pVDZ level for both conformers of each species are collected in Table 1 together with their population fractions (given as Boltzmann percentage weights, 100 X_i) in both the gas phase and solvents.

DISCUSSION

We begin with a discussion of the results for the Boltzmann populations given in Table 1.

For compound **2**, both conformers are approximately equally populated, with conformer **c2** prevailing over **c1** in the gas phase and in acetonitrile, and the opposite occurring in methanol. The population of conformer **c1** is thus seen to increase with increased polarity of the solvent, with the opposite occurring for conformer **c2**. Compound **3** is predominantly found as **c1** in vacuo; it is basically equally distributed between the two conformers in acetonitrile and it prevails as **c2** in methanol. Increasing the polarity of the solvent, the population of **c1** decreases and that of **c2** increases. These differences in population distribution slightly affect the resulting absolute value of the specific optical rotation, but they have no effect on its resulting sign because both conformers have negative specific rotations (Table 2).

For both DFT functionals and in all three environments (vacuum, methanol, and acetonitrile), the total specific optical rotation of the two investigated dihydropyridazines is thus opposite to the experimentally measured specific rotation. In absolute value, the computed rotations of compound **2** are roughly three times larger than the experimental ones when using the B3LYP functional, and they are twice as large when using CAMB3LYP. For compound **3**, the differences are slightly reduced but are always around twice as large. Despite

Table 1. Gibbs Free Energies (in Hartree) and Boltzmann Percentage Weights at T = 298.15 K[a]

compound 2						
	gas phase		CH_3CN		CH_3OH	
	2-c1	**2-c2**	**2-c1**	**2-c2**	**2-c1**	**2-c2**
G_i^0	−763.623370	−763.623480	−763.636483	−763.636505	−763.636432	−763.636431
100 X_i	47.09	52.91	49.42	50.58	50.03	49.97
compound 3						
	gas phase		CH_3CN		CH_3OH	
	3-c1	**3-c2**	**3-c1**	**3-c2**	**3-c1**	**3-c2**
G_i^0	−3337.195139	−3337.193349	−3337.206340	−3337.206322	−3337.215200	−3337.215882
100 X_i	86.94	13.06	50.48	49.52	32.69	67.31

[a]B3LYP results in the aug-cc-pVDZ basis set.

dx.doi.org/10.1021/jo401343y | J. Org. Chem. 2013, 78, 11670−11679

Table 2. Calculated Specific Optical Rotation $[\alpha]_D$ (degrees cm^2 g^{-1}) at the Sodium D-line and Comparison with Experimental Results

	compound 2					
	B3LYP/aug-cc-pVDZ			CAMB3LYP/aug-cc-pVDZ		
	gas phase	CH_3CN	CH_3OH	gas phase	CH_3CN	CH_3OH
2-c1	−1122.63	−1304.84	−1302.32	−868.52	−1009.99	−1007.61
2-c2	−767.77	−1375.47	−1373.19	−620.32	−1055.23	−1053.76
averaged	−934.88	−1340.57	−1337.74	−737.20	−1032.87	−1030.67
expt (at 20 °C) ee 46%			+211.2 (+459.1[a])			+211.2 (+459.1[a])
	compound 3					
	B3LYP/aug-cc-pVDZ			CAMB3LYP/aug-cc-pVDZ		
	gas phase	CH_3CN	CH_3OH	gas phase	CH_3CN	CH_3OH
3-c1	−1026.98	−1149.84	−1174.68	−789.01	−893.07	−902.80
3-c2	−621.76	−1179.68	−1178.14	−503.31	−897.96	−896.30
averaged	−974.06	−1164.62	−1177.01	−751.70	−895.50	−898.42
expt (at 25 °C) ee 72%			+404.4 (+561.7[a])			+404.4 (+561.7[a])

[a]Computed experimental value at a hypothetical 100% enantiomeric excess.

Table 3. Excitation Frequencies, ω_{gf} (eV), and Corresponding Wavelengths, λ_{gf} (nm), OPA Oscillator Strengths, δ_{OPA} (au), and ECD Rotatory Strengths, R_{ECD} (au), of the First 15 Excited States of Conformers c1 and c2 Calculated at the B3LYP/aug-cc-pVDZ and CAMB3LYP/aug-cc-pVDZ Levels in Methanol for Compound 2

		B3LYP				CAMB3LYP			
		ω_{gf}	λ_{gf}	$\delta_{OPA} \times 10^2$	$R_{ECD} \times 10^2$	ω_{gf}	λ_{gf}	$\delta_{OPA} \times 10^2$	$R_{ECD} \times 10^2$
2-c1	S_1	3.8578	321.42	11.81	−9.5637	4.1525	298.62	14.76	−11.50
	S_2	4.5735	271.13	5.2411	−9.7507	5.1712	239.79	2.3584	−9.0787
	S_3	4.7695	260.09	0.61248	−1.6325	5.2884	234.48	0.24566	1.3224
	S_4	4.8550	255.41	3.0468	0.83484	5.4920	225.78	1.9264	0.088247
	S_5	4.9023	252.94	0.62061	1.9988	5.5067	225.18	3.8706	−0.44482
	S_6	4.9623	249.88	7.2750	−3.0826	5.6719	218.62	14.95	−9.2981
	S_7	4.9892	248.54	0.37346	−1.9654	5.8029	213.69	5.0147	10.60
	S_8	5.3637	231.19	4.1204	−0.0276	5.9349	208.93	4.2847	−1.5878
	S_9	5.3752	230.69	0.96206	1.8478	6.0306	205.62	1.4766	2.4537
	S_{10}	5.4187	228.84	1.7012	−0.0345	6.1633	201.19	1.4765	−0.29283
	S_{11}	5.5138	224.89	0.10416	−0.0051	6.1946	200.17	2.5304	0.68362
	S_{12}	5.6015	221.37	0.66246	2.5422	6.2200	199.36	8.8661	−3.4469
	S_{13}	5.6846	218.13	1.3754	3.8427	6.3149	196.36	8.5070	6.3605
	S_{14}	5.7607	215.25	5.0482	−3.3363	6.3626	194.89	0.56090	2.3233
	S_{15}	5.8388	212.37	1.6744	0.63091	6.4390	192.58	3.2106	2.5959
2-c2	S_1	3.8687	320.52	12.41	−11.35	4.1556	298.40	15.07	−12.18
	S_2	4.5908	270.10	5.7205	−6.7226	5.2601	235.74	2.2790	−3.8718
	S_3	4.8050	258.06	1.3216	−1.7921	5.3467	231.92	2.6834	−5.5989
	S_4	4.8619	255.04	0.31688	−1.0285	5.4701	226.69	3.8229	2.8818
	S_5	4.9044	252.83	7.5647	3.7223	5.5179	224.72	1.2808	2.1757
	S_6	4.9878	248.61	0.89961	−1.9263	5.6581	219.16	12.71	−9.3654
	S_7	5.0041	247.80	0.72354	−2.6961	5.8123	213.34	3.3754	8.3091
	S_8	5.3514	231.71	1.3887	−1.5790	5.9511	208.36	5.0478	−1.8445
	S_9	5.3655	231.10	2.0993	2.1445	6.0133	206.21	2.2759	3.6560
	S_{10}	5.4750	226.49	0.51523	0.80488	6.1671	201.07	6.4770	0.89718
	S_{11}	5.4936	225.72	0.18196	0.44729	6.1742	200.84	0.03218	−0.03651
	S_{12}	5.5563	223.17	2.0790	5.7758	6.2309	199.01	2.7726	−1.2000
	S_{13}	5.6831	218.19	1.7002	3.8345	6.2818	197.39	7.8537	8.5595
	S_{14}	5.7474	215.75	5.6817	−4.3976	6.3635	194.86	0.54948	2.2572
	S_{15}	5.8446	212.16	1.6702	1.1061	6.4415	192.50	1.7527	3.1432

these remarkable differences, we are not concerned with the absolute value of the rotation but only with its sign. Even assuming that our results are in error by as much as 50% (an error that is much larger than what is commonly attributed to TDDFT OR calculations using the chosen functionals[21] or than what one can expect to arise from our neglect of vibrational effects[22] and the use of a "basic" PCM description of solvent effects instead of more sophisticated ones[23] and bearing in mind that we are dealing with a large chiro-optical response), the sign of our rotations is unambiguously negative and yields

dx.doi.org/10.1021/jo401343y | J. Org. Chem. 2013, 78, 11670−11679

Table 4. Excitation Frequencies, ω_{gf} (eV), and Corresponding Wavelengths, λ_{gf} (nm), OPA Oscillator Strengths, δ_{OPA} (au), and ECD Rotatory Strengths, R_{ECD} (au), of the First 15 Excited States of Conformers c1 and c2 Calculated at the B3LYP/aug-cc-pVDZ and CAMB3LYP/aug-cc-pVDZ Levels in Methanol for Compound 3

		B3LYP				CAMB3LYP			
		ω_{gf}	λ_{gf}	$\delta_{OPA} \times 10^2$	$R_{ECD} \times 10^2$	ω_{gf}	λ_{gf}	$\delta_{OPA} \times 10^2$	$R_{ECD} \times 10^2$
3-c1	S_1	3.8245	324.23	10.71	−10.57	4.1374	299.70	14.48	−13.23
	S_2	4.4914	276.08	0.49745	−0.69274	5.1346	241.50	4.0737	−9.3338
	S_3	4.5182	274.45	9.9894	−11.55	5.1862	239.09	1.3513	−1.5711
	S_4	4.7068	263.45	7.0012	−4.7255	5.4091	229.24	8.7986	−2.0502
	S_5	4.8584	255.23	3.8558	0.91308	5.4812	226.23	1.5005	−1.1888
	S_6	4.9338	251.33	0.49800	−0.67841	5.5008	225.42	8.5952	−5.9412
	S_7	4.9523	250.39	1.3155	−0.012905	5.5249	224.44	8.1540	4.8709
	S_8	5.1296	241.73	0.009882	−0.098118	5.6153	220.83	4.7334	−1.7019
	S_9	5.1716	239.77	0.24808	0.26869	5.8169	213.17	12.76	6.2129
	S_{10}	5.3545	231.58	2.2421	−0.93730	5.9669	207.81	3.3637	2.0914
	S_{11}	5.3839	230.32	7.5591	5.2137	6.1871	200.42	0.79917	0.13292
	S_{12}	5.4659	226.86	1.3225	−0.22214	6.2055	199.82	1.9147	0.30714
	S_{13}	5.4980	225.54	15.90	−1.2786	6.2300	199.04	9.3918	1.4441
	S_{14}	5.5359	223.99	3.6292	3.4629	6.3080	196.58	2.1674	2.3097
	S_{15}	5.5547	223.23	0.05676	−0.20582	6.3355	195.72	14.45	6.3967
3-c2	S_1	3.8377	323.11	10.96	−0.1135	4.1481	298.93	14.43	−12.79
	S_2	4.5105	274.92	6.1253	−5.1108	5.1528	240.64	1.8486	−2.5063
	S_3	4.5464	272.74	5.6402	−4.9123	5.2975	234.07	12.96	−0.1139
	S_4	4.7460	261.27	8.7809	−0.93441	5.4435	227.79	6.6809	8.2720
	S_5	4.9170	252.19	0.17229	−0.48414	5.4956	225.63	6.6260	−10.54
	S_6	4.9693	249.53	0.90661	−2.5869	5.4982	225.53	0.19639	−0.2289
	S_7	4.9868	248.66	1.2215	−0.2585	5.5513	223.37	2.1898	3.8185
	S_8	5.1441	241.05	0.006792	−0.054178	5.6390	219.90	4.8445	−2.5668
	S_9	5.2014	238.40	0.28262	0.15330	5.8124	213.34	15.81	5.4628
	S_{10}	5.3269	232.78	2.0070	−0.71408	5.9708	207.68	2.4957	2.3984
	S_{11}	5.3796	230.50	3.8253	2.5089	6.1908	200.30	3.3204	3.7915
	S_{12}	5.4724	226.59	13.82	4.8840	6.2135	199.57	3.4052	1.5588
	S_{13}	5.5037	225.30	8.9061	−0.29844	6.2482	198.46	2.9103	−0.7041
	S_{14}	5.5402	223.82	1.8460	1.6728	6.3070	196.61	5.2135	7.9971
	S_{15}	5.5548	223.23	0.13154	0.15546	6.3212	196.17	10.51	2.7881

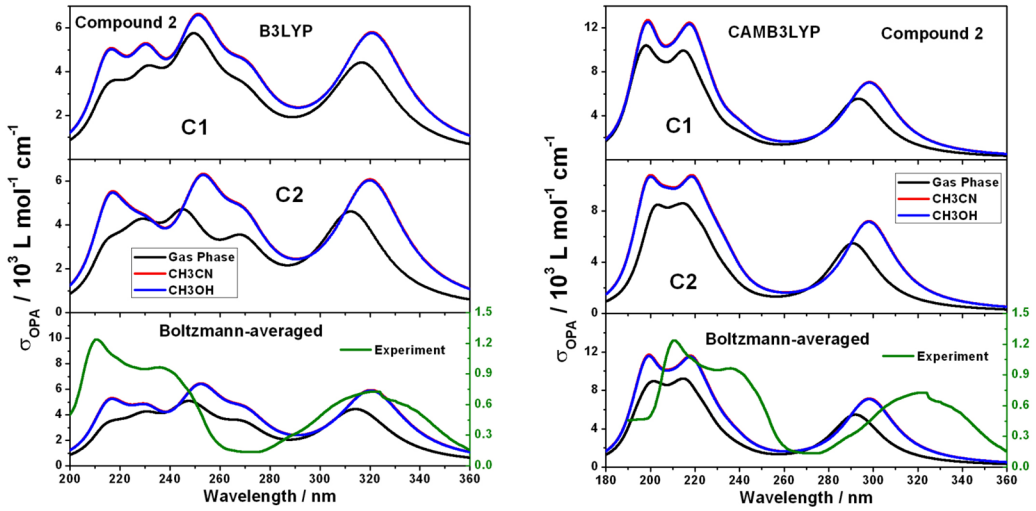

Figure 5. Compound **2.** Calculated OPA of the two conformers, **c1** (top panels) and **c2** (middle panels), at both the B3LYP/aug-cc-pVDZ (left) and CAMB3LYP/aug-cc-pVDZ (right) levels. The spectra were obtained by convoluting the first 15 excited states with a Lorentzian broadening lifetime of 0.2 eV both in vacuo (black lines) as well as in methanol (blue lines) and acetonitrile (red lines, basically overlapping the blue ones). Boltzmann-averaged spectra are given in the bottom panels. The experimental spectrum (given as dimensionless absorbance) recorded in methanol is also shown in the bottom panels (green curve, magnitude on the right axis).

dx.doi.org/10.1021/jo401343y | J. Org. Chem. 2013, 78, 11670−11679

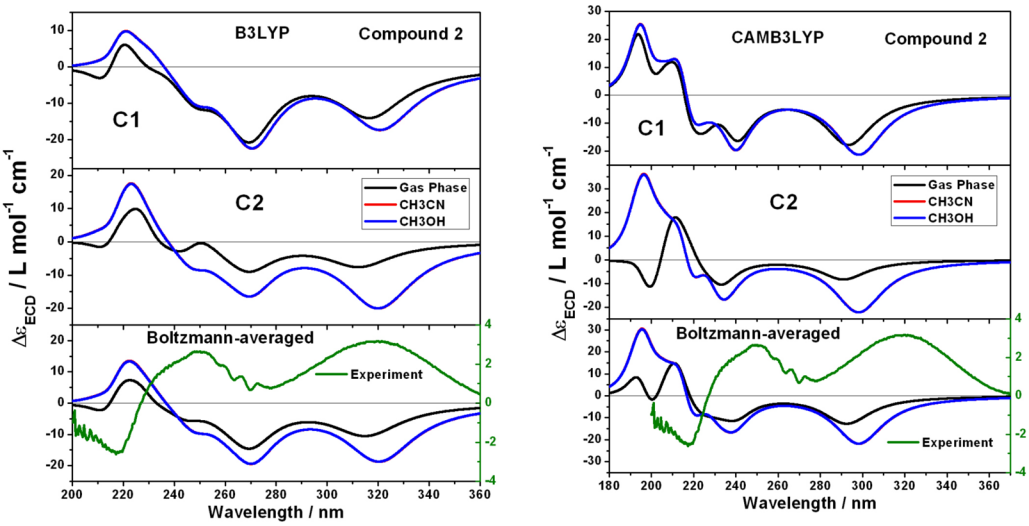

Figure 6. Compound **2.** Calculated ECD of the two conformers, **c1** (top panels) and **c2** (middle panels), at both the B3LYP/aug-cc-pVDZ (left) and CAMB3LYP/aug-cc-pVDZ (right) levels. The spectra were obtained by convoluting the rotational strengths of the first 15 excited states with a Lorentzian broadening lifetime of 0.2 eV both in vacuo (black lines) as well as in methanol (blue lines) and acetonitrile (red lines, basically overlapping the blue ones). Boltzmann-averaged spectra are given in the bottom panels. The experimental spectrum (recorded in methanol) is also shown in the bottom panels (green lines, magnitude scale on the right axis).

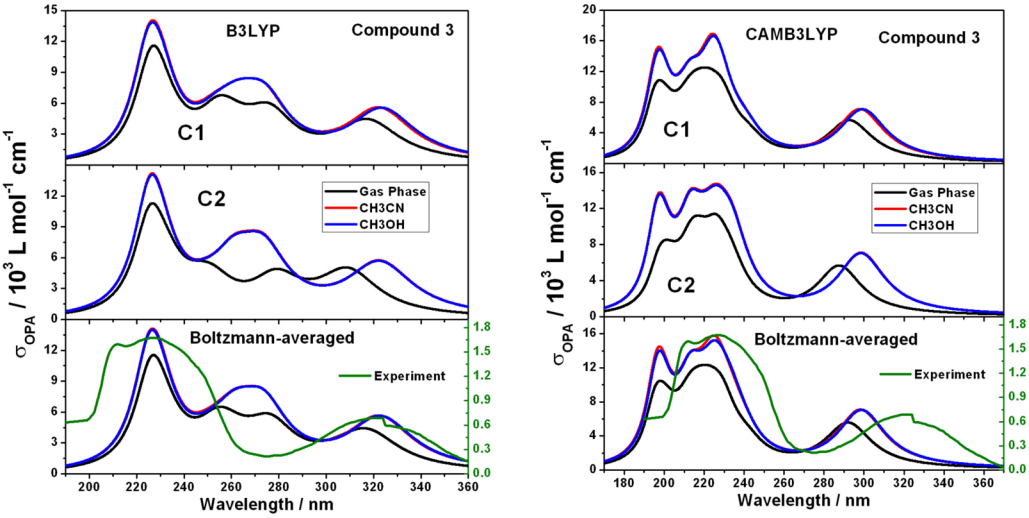

Figure 7. Compound **3**. Calculated OPA of the two conformers, **c1** (top panels) and **c2** (middle panels), at both the B3LYP/aug-cc-pVDZ (left) and CAMB3LYP/aug-cc-pVDZ (right) levels of theory. The spectra were obtained by convoluting the transition strengths of the first 15 excited states with a Lorentzian broadening lifetime of 0.2 eV both in vacuo (black lines) as well as in methanol (blue lines) and acetonitrile (red lines, basically overlapping the blue ones). Boltzmann-averaged spectra are given in bottom panels. The experimental spectrum recorded in methanol, given as dimensionless absorbance, is also shown in the bottom panels (green lines, magnitude scale on the right axis).

the conclusion that the two selected 1,4-dihydropyridazines have been synthesized in the (*R*) absolute configuration, and not (*S*), as previously postulated[13] on the basis of the generally accepted catalytic mechanism of L-proline.

As anticipated, because the determination of the ac based on the sign of the OR alone could be disputable,[24] we have also performed computations of the ECD spectra (along with the OPA ones) of both species. In Tables 3 and 4, we collect the results (in methanol) for the excitation energies (ω_{gf}), oscillator strengths for OPA (δ_{OPA}), and rotation strengths for ECD (R_{ECD}) for the first 15 excited states of the two conformers of compounds **2** and **3**, respectively.

The computed OPA spectra of the two conformers of compound **2** are shown in Figure 5 at both the B3LYP and CAMB3LYP levels of theory. The Boltzmann-averaged spectra are given in the bottom panels together with the corresponding experimental spectrum in methanol (green line) for comparison. As can be appreciated from the figures, introduction of solvent effects slightly affects both the peak position (red-shifted) and intensity (enhanced) with respect to the gas phase, whereas the differences between the results in the two different solvents applied here (CH_3CN and CH_3OH) are practically negligible. The latter is consistent with what was observed experimentally.

The experimental OPA spectrum shows three absorption bands: one, rather broad, band stretching from 360 to 280 nm centered at around 323 nm (relative intensity 0.728) and two narrower overlapping bands peaked at 236 (intensity 0.965) and 211 nm (intensity 1.237). After performing the Boltzmann-average, as indicated in the bottom panels, B3LYP reproduced

dx.doi.org/10.1021/jo401343y | J. Org. Chem. 2013, 78, 11670−11679

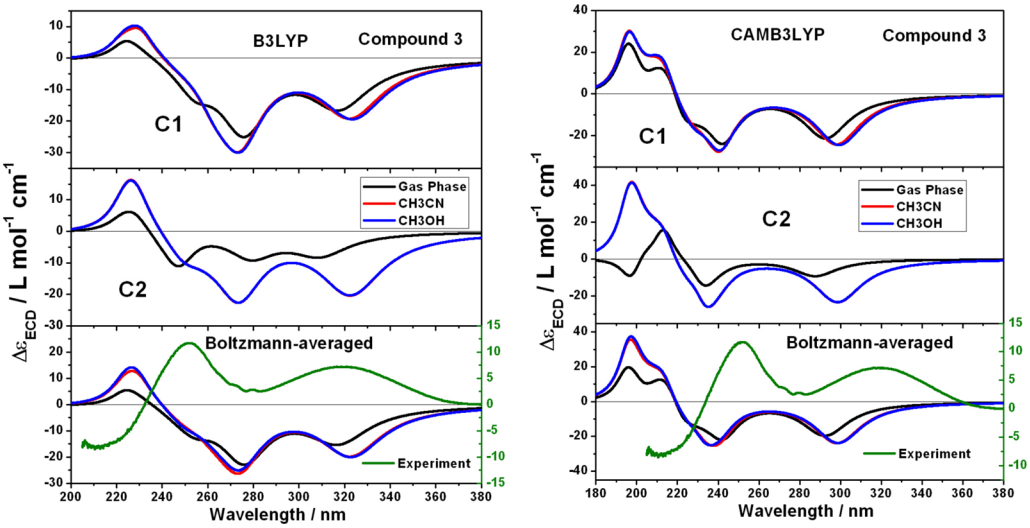

Figure 8. Compound **3**. Calculated ECD spectra of the two conformers, **c1** (top panels) and **c2** (middle panels), at the both B3LYP/aug-cc-pVDZ (left) and CAMB3LYP/aug-cc-pVDZ (right) levels. The spectra were obtained by convoluting the rotational strengths of the first 15 excited states with a Lorentzian broadening lifetime of 0.2 eV both in vacuo (black lines) as well as in methanol (blue lines) and acetonitrile (red lines, basically overlapping the blue ones). Boltzmann-averaged spectra are given in the bottom panels. The experimental spectrum (recorded in methanol) is also shown in the bottom panels (green lines, magnitude scale on the right-axis).

Scheme 1

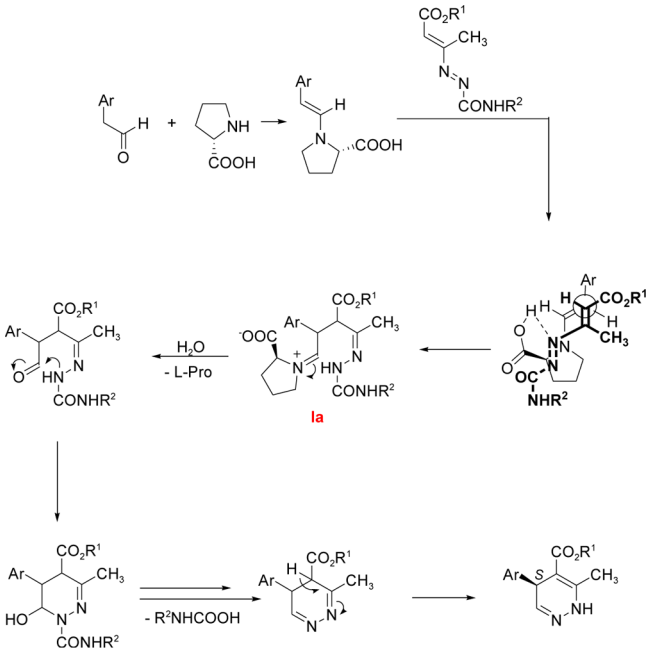

very well the experimental broad band (centered at 323 nm), which is consistent with the first computed excited state S_1 found around 321.42 (**2-c1**) and 320.52 nm (**2-c2**) (Table 3). The relative distance from the other bands is, however, underestimated. With the adopted Lorentzian lifetime of 0.2 eV, five bands emerge in the B3LYP spectrum instead of three major bands like in the experiment. As one can see from the results in Table 3, the band centered at ~270 nm is resulting from the S_2 state for both conformers, whereas the remaining bands are actually from a combined contribution of many states.

The CAMB3LYP functional reproduces well the three peaks seen in the experimental spectrum as well as the relative distance between the first and second peak, but it does so with a slight underestimation of the intensity and relative position of the third peak on the blue-end, which might be ascribed to the contribution of higher states out of our consideration. Moreover, all of the peaks are blue-shifted (toward higher energy) with respect to the experiment. For example, the first broad band occurs at around 298 nm after Boltzmann-average, which shows a 25 nm blue shift by comparison with the experiment.

Figure 6 shows the computed ECD spectra of 1,4-dihydropyridazine **2**. Also for the ECD spectrum, the two conformers of **2** have rotational strengths of equal sign for the two lowest-energy transitions, which frees us from potential problems related to the cancellation of errors between oppositely signed signals. Convolution of the rotational strengths with the line shape functions, as described in the previous section, and Boltzmann average yields the spectrum given in the bottom panel of Figure 6, which is compared vis-a-vis with the experimental spectrum (green line). Despite the relatively contained shift of the peaks because of the observed shifts in the excitation energies described above, the two dominant peaks in the wavelength region 200−350 nm are clearly opposite to the experimental peaks, confirming our assignment of the absolute configuration of **2** on the basis of the OR results as (*R*) and not (*S*).

In the case of compound **3** (Figure 7) the experimental OPA spectrum recorded in methanol shows a broad band (370−270 nm) with maximum estimated at 321 nm with absorbance 0.691 and two almost completely overlapping bands with peaks at 227 (absorbance 1.673) and 210 nm (absorbance 1.596). Similar to what was observed for compound **2**, the first absorption band is consistent with our computed first excited state, whose position is very well reproduced by B3LYP at around 321.42 nm for **3-c1** and 320.52 nm for **3-c2**. With CAMB3LYP, however, the first excitation once again is blue-shifted (higher energy) and occurs at around 298−299 nm. The two overlapping bands are better reproduced by CAMB3LYP; their relative distance is significantly overestimated by B3LYP. Thus, despite the overall blue shift of the whole spectrum,

dx.doi.org/10.1021/jo401343y | J. Org. Chem. 2013, 78, 11670−11679

Scheme 2

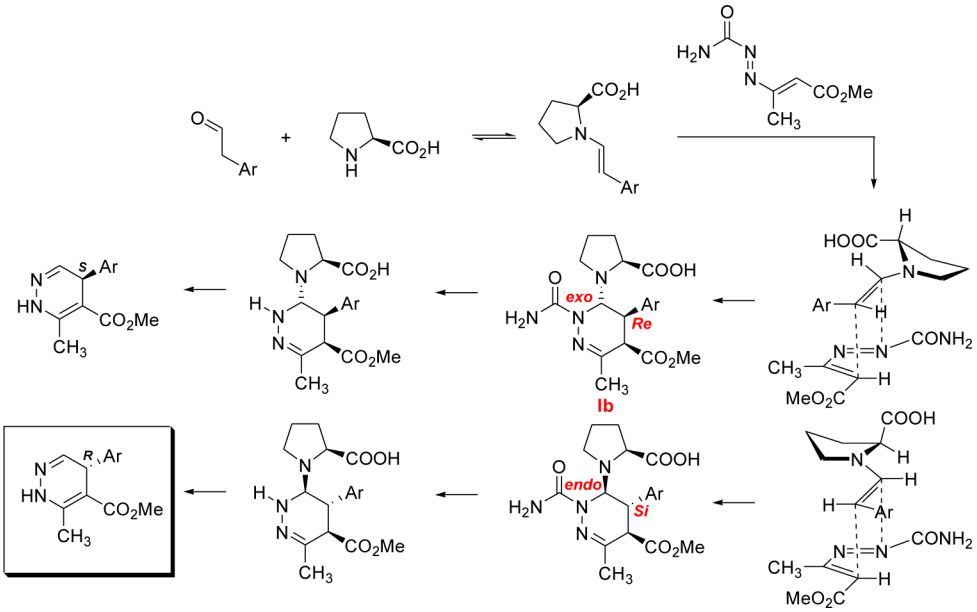

CAMB3LYP yields a somewhat better agreement with the experimental profiles.

The computed rotational strengths of 1,4-dihydropyridazine **3** (Figure 8) are, analogously to what was observed for compound **2**, of equal sign for the two lowest-energy transitions, yielding, after convolution and Boltzmann average, the spectrum given in the bottom panel of Figure 8, which is compared to the experimental spectrum. The two dominant peaks in this case are also opposite to the experimental peaks, further validating our assignment of the absolute configuration of **3** on the basis of the OR results as (R) and not (S).

To conclude this section, a comment on the neglect of vibrational effects on the ECD spectra is in place. Vibrations can, in principle, introduce a change of sign for some systems because of the Herzberg–Teller contribution.[22c] This possibility can be estimated by inspecting the layout of the excited-state manifold because the general behavior of the Herzberg–Teller contribution can be rationalized by its well-known borrowing mechanism, that is, it originates from the coupling between states (borrowing intensity from neighboring states). In general, the necessary precondition for a strong Herzberg–Teller contribution to a given excited state is the presence of other strong states close by in energy. By inspecting Table 3, for instance, the CAMB3LYP results, the first two states give very strong negative signals, which means that Franck–Condon dominates for these two states, with negligible contributions from Herzberg–Teller effects. S_3 shows a much smaller positive peak, and it could, in principle, manifest strong Herzberg–Teller effects that, however, are expected to be negative because the state can borrow intensity from its two strong neighbors, S_1 and S_2, which are both negative. Even if there is a possibility for sign change for S_3 (from positive to negative) if one considers the whole range covering the first three states, there is no possibility for a sign reversal of the two main peaks from negative to positive.

Reaction Mechanisms and Stereospecificity. On the basis of the results of the computational investigation of the specific optical rotation at the sodium D-line and of the ECD spectra of the two chiral 1,4-dihydropyridazines discussed above, we have now assigned the absolute configuration as (*R*). This is opposite to the one tentatively assigned in our previous paper[13] by consideration of the generally accepted reaction mechanism for the organocatalyst used. The latter was based on a regioselective Michael-type reaction of the *β*-carbon atom of the enamine to the electrophilic terminal carbon atom of the azo-ene system (Scheme 1).

In our opinion, this means that we have to hypothesize that a different mechanism is acting in the organocatalyzed reaction.

Another type of reaction that can be effective with 1,2-diaza-1,3-dienes, particularly in the presence of electron-withdrawing groups on the terminal atoms of the azo-ene system, is the inverse electron demand aza Diels–Alder reaction. Chen and co-workers[25] suggested this type of mechanism for the reactions of *N*-sulfonyl-1-aza-1,3-butadienes and electron-rich alkenes in the presence of *α*,*α*-diphenylprolinoltrimethylsilyl ether. On these grounds, we consider here a second possible mechanism, which is illustrated in Scheme 2.

A closely similar mechanism has been proposed in the addition of enamines derived from prolinol to nitro olefins.[26] A DFT evaluation of this reaction has been carried out by Pihko and co-workers,[27] and a zwitterionic intermediate, corresponding to intermediate **Ia** in the reaction path depicted in Scheme 1, could not be located as a low-lying energy minimum on the potential energy surface even with the inclusion of solvent effects. We have performed an initial analysis on the main intermediates of our two alternative reaction paths **Ia** (Scheme 1) and **Ib** (Scheme 2) by optimizing the geometries of the whole set of their diastereoisomers at the B3LYP/6-31G(d,p) level of theory. We find that intermediates **Ib** are by far lower in energy than intermediates **Ia** (the difference is 24 kcal/mol). Even if our reaction is carried out in THF, whereas the calculations were performed in gas phase, such a large energy difference is likely to be reduced, but not reverted, in the relatively low-polarity environment provided by the excess reactant molecules along the reaction. Further computational studies are in any case being performed to verify such assumption. We can therefore agree with Pihko and rule out the zwitterion intermediate **Ia** also from our picture. As to the

dx.doi.org/10.1021/jo401343y | J. Org. Chem. 2013, 78, 11670–11679

enantioselectivity, we have found a very small energy difference between the *endo* and *exo* intermediates **Ib**, in favor of the *exo* geometry by only 0.7 kcal/mol. A very small difference is actually expected from the experimental data, as a 70% enantiomeric excess at room temperature would mean a difference of just 0.82 kcal/mol in the rate-determining activation barriers of the two diastereomeric paths. This value could be barely reproduced in DFT calculations, being less than the usual accuracy of DFT predictions of activation barriers in pericyclic reactions: Seebach and colleagues[26] have found and discussed this in evaluating the stereoselectivity of enamine addition to nitro olefins, and the general topic has been reviewed by Ess, Jones, and Houk.[28] Therefore, we believe that our preliminary analysis supports the aza Diels–Alder mechanisms. However, the ultimate evidence would be given by the isolation of intermediate **Ib** from a stoichiometric reaction between the enamine and the azodiene, a task that goes beyond the scopes of the investigation reported here.

Summary and Concluding Remarks. A computational investigation at the (TD)DFT level of theory of the specific optical rotation at the sodium D-line and of the ECD spectra of two chiral 1,4-dihydropyridazines, previously synthesized in our group, was carried out to confirm the assignment of their absolute configuration based on the reaction mechanism of the organocatalyst used for their synthesis. The computational results clearly indicate that the absolute configuration is opposite to the one previously postulated and therefore a different reaction mechanism must be taken into account to explain this outcome. An inverse electron demand Diels–Alder reaction is likely to be a correct alternative, as indicated by the calculations performed on the intermediates of the two possible mechanisms. In fact, the intermediate of the inverse electron demand Diels–Alder mechanism is by far lower in energy than the intermediate of the Michael-type mechanism (>24 kcal/mol). Unfortunately, DFT calculations at present do not allow us to discriminate between the two enantiomeric approaches.

■ ASSOCIATED CONTENT

Supporting Information

Definitions and working equations of the computed properties as well as Cartesian coordinates and absolute energies of all species considered. This material is available free of charge via the Internet at http://pubs.acs.org.

■ AUTHOR INFORMATION

Corresponding Author

*E-mail: coriani@units.it.

Notes

The authors declare no competing financial interest.

■ ACKNOWLEDGMENTS

We acknowledge financial support from the National Nature Science Foundation of China (grant no. 21003085), the Ministero dell'Istruzione, dell'Università e della Ricerca (MIUR) (PRIN projects: 2010FPTBSH_005, NANO Molecular tEchnologies for Drug delivery – NANOMED, and 2009C28YBF_001, Modelli teorici per processi di fotoassorbimento e fotoemissione), and the University of Trieste (Fondo per la Ricerca d'Ateneo, FRA 2012).

■ REFERENCES

(1) Frankowiak, G.; Meyer, H.; Bossert, F.; Heise, A.; Kazda, S.; Stoepel, K.; Towart, R.; Wehinger, E. Patent US 4,348,395, 1982

(2) (a) Loev, B.; Jones, H.; Shroff, J. R. Patent US 4,435,395, 1984. (b) Testa, R.; Leonardi, A.; Tajana, A.; Riscassi, E.; Magliocca, R.; Sartani, A. *Cardiovasc. Drug Rev.* **1997**, *15*, 187–219.

(3) Chiou, G. C.; Yao, Q. S.; Okawara, T. *J. Ocul. Pharmacol.* **1994**, *10*, 577–586.

(4) (a) Potikha, L. M.; Kovtunenko, V. A.; Turov, A. V. *Chem. Heterocycl. Compd.* **2009**, *45*, 815–822. (b) Ghozlan, S. A. S.; Mohamed, M. H.; Abdelmoniem, A. M.; Abdelhamid, I. A. *ARKIVOC* **2009**, 302–311. (c) Cecchi, M.; Micoli, A.; Giomi, D. *Tetrahedron* **2006**, *62*, 12281–12287. (d) Yakovlev, M. E.; Razin, V. V. *Russ. J. Org. Chem.* **2004**, *40*, 1033–1036.

(5) (a) Potikha, L. M.; Kovtunenko, V. A.; Turov, A. V.; Palamarchuk, G. V.; Zubatyuk, R. I.; Shishkin, O. V. *Chem. Heterocycl. Compd.* **2009**, *45*, 327–335. (b) Bakkali, H.; Marie, C.; Ly, A.; Thobie-Gautier, C.; Graton, J.; Pipelier, M.; Sengmany, S.; Leonel, E.; Nedelec, J.-Y.; Evain, M.; Dubreuil, D. *Eur. J. Org. Chem.* **2008**, 2156–2166.

(6) Özer, G.; Saracoglu, N.; Menzek, A.; Balci, M. *Tetrahedron* **2005**, *61*, 1545–1550.

(7) Xie, H.; Zhu, J.; Chen, Z.; Li, S.; Wu, Y. *Synlett* **2012**, *23*, 935–937.

(8) (a) Razin, V. V.; Yakovlev, M. E.; Vasin, V. A. *Russ. J. Org. Chem.* **2012**, *48*, 434–438. (b) Razin, V. V.; Yakovlev, M. E.; Shataev, K. V.; Selivanov, S. I. *Russ. J. Org. Chem.* **2004**, *40*, 1027–1032.

(9) (a) Al-Mousawi, S. M.; Moustafa, M. S.; Elnagdi, M. H. *Heterocycles* **2008**, *75*, 2201–2211. (b) Ghozlan, S. A. S.; Abdelhamid, I. A.; Hassaneen, H. M.; Elnagdi, M. H. *J. Heterocycl. Chem.* **2007**, *44*, 105–108.

(10) (a) Rusinov, G. L.; Ishmetova, R. I.; Latosh, N. I.; Ganebnych, I. N.; Chupakhin, O. N.; Potemkin, V. A. *Russ. Chem. Bull.* **2000**, *49*, 355–362. (b) Pindur, U.; Kim, M.-H. *Tetrahedron Lett.* **1988**, *29*, 3927–3928. (c) Sauer, J.; Heinrichs, G. *Tetrahedron Lett.* **1966**, *41*, 4979–4984.

(11) Marek, R.; Potáček, M.; Sapík, M. *Tetrahedron Lett.* **1995**, *36*, 8101–8102.

(12) Buonora, P. T.; Zhang, Q.; Sawko, J.; Westrum, L. J. *Tetrahedron: Asymmetry* **2008**, *19*, 27–30.

(13) Pitacco, G.; Attanasi, O. A.; De Crescentini, L.; Favi, G.; Felluga, F.; Forzato, C.; Mantellini, F.; Nitti, P.; Valentin, E.; Zangrando, E. *Tetrahedron: Asymmetry* **2010**, *21*, 617–622.

(14) (a) List, B.; Hoang, L.; Martin, H. J. *Proc. Natl. Acad. Sci. U.S.A.* **2004**, *101*, 5839–5842. (b) Okuyama, Y.; Nakano, H.; Watanabe, Y.; Makabe, M.; Takeshita, M.; Uwai, K.; Kabuto, C.; Kwong, E. *Tetrahedron Lett.* **2009**, *50*, 193–197.

(15) (a) Becke, A. D. *Phys. Rev. A* **1988**, *38*, 3098–3100. (b) Becke, A. D. *J. Chem. Phys.* **1993**, *98*, 5648–5652. (c) Lee, C.; Yang, W.; Parr, R. G. *Phys. Rev. B* **1988**, *37*, 785–789.

(16) (a) Miertuš, S.; Scrocco, E.; Tomasi, J. *Chem. Phys.* **1981**, *55*, 117–129. (b) Tomasi, J.; Mennucci, B.; Cammi, R. *Chem. Rev.* **2005**, *105*, 2999–3093.

(17) Frisch, M. J.; Trucks, G. W.; Schlegel, H. B.; Scuseria, G. E.; Robb, M. A.; Cheeseman, J. R.; Montgomery, J. A.; Jr.; Vreven, T.; Kudin, K. N.; Burant, J. C.; Millam, J. M.; Iyengar, S. S.; Tomasi, J.; Barone, V.; Mennucci, B.; Cossi, M.; Scalmani, G.; Rega, N.; Petersson, G. A.; Nakatsuji, H.; Hada, M.; Ehara, M.; Toyota, K.; Fukuda, R.; Hasegawa, J.; Ishida, M.; Nakajima, T.; Honda, Y.; Kitao, O.; Nakai, H.; Klene, M.; Li, X.; Knox, J. E.; Hratchian, H. P.; Cross, J. B.; Bakken, V.; Adamo, C.; Jaramillo, J.; Gomperts, R.; Stratmann, R. E.; Yazyev, O.; Austin, A. J.; Cammi, R.; Pomelli, C.; Ochterski, J. W.; Ayala, P. Y.; Morokuma, K.; Voth, G. A.; Salvador, P.; Dannenberg, J. J.; Zakrzewski, V. G.; Dapprich, S.; Daniels, A. D.; Strain, M. C.; Farkas, O.; Malick, D. K.; Rabuck, A. D.; Raghavachari, K.; Foresman, J. B.; Ortiz, J. V.; Cui, Q.; Baboul, A. G.; Clifford, S.; Cioslowski, J.; Stefanov, B. B.; Liu, G.; Liashenko, A.; Piskorz, P.; Komaromi, I.; Martin, R. L.; Fox, D. J.; Keith, T.; Al-Laham, M. A.; Peng, C. Y.; Nanayakkara, A.; Challacombe, M.; Gill, P. M. W.; Johnson, B.; Chen,

W.; Wong, M. W.; Gonzalez, C.; Pople, J. A. *Gaussian 03*, revision D.01; Gaussian, Inc.: Wallingford, CT, 2004.
(18) (a) Yanai, Y.; Tew, D. P.; Handy, N. C. *Chem. Phys. Lett.* **2004**, *393*, 51−57. (b) Peach, M. J. G.; Helgaker, T.; Salek, P.; Keal, T. W.; Lutnaes, O. B.; Tozer, D. J.; Handy, N. C. *Phys. Chem. Chem. Phys.* **2006**, *8*, 558−562.
(19) Aidas, K.; Angeli, C.; Bak, K. L.; Bakken, V.; Bast, R.; Boman, L.; Christiansen, O.; Cimiraglia, R.; Coriani, S.; Dahle, P.; Dalskov, E. K.; Ekström, U.; Enevoldsen, T.; Eriksen, J. J.; Ettenhuber, P.; Fernàndez, B.; Ferrighi, L.; Fliegl, H.; Frediani, L.; Hald, K.; Halkier, A.; Hättig, C.; Heiberg, H.; Helgaker, T.; Hennum, A. C.; Hettema, H.; Høst, S.; Høyvik, I.-M.; Iozzi, M. F.; Jansik, B.; Jensen, H. J. A.; Jonsson, D.; Jørgensen, P.; Kauczor, J.; Kirpekar, S.; Kjærgaard, T.; Klopper, W.; Knecht, S.; Kobayashi, R.; Koch, H.; Kongsted, J.; Krapp, A.; Kristensen, K.; Ligabue, A.; Lutnæs, O. B.; Melo, J. I.; Mikkelsen, K. V.; Myhre, R. H.; Neiss, C.; Nielsen, C. B.; Norman, P.; Olsen, J.; Olsen, J. M. H.; Osted, A.; Packer, M. J.; Pawlowski, F.; Pedersen, T. B.; Provasi, P. F.; Reine, S.; Rinkevicius, Z.; Ruden, T. A.; Ruud, K.; Rybkin, V.; Salek, P.; Samson, C. C. M.; Sànchez de Meràs, A.; Saue, T.; Sauer, S,P.A.; Schimmelpfennig, B.; Sneskov, K.; Steindal, A. H.; Sylvester-Hvid, K. O.; Taylor, P. R.; Teale, A. M.; Tellgren, E. I.; Tew, D. P.; Thorvaldsen, A. J.; Thøgersen, L.; Vahtras, O.; Watson, M.; Wilson, D. J.; Ziolkowski, M.; Ågren, H. *WIREs Comput. Mol. Sci.* **2013**, DOI: 10.1002/wcms.1172.
(20) (a) Autschbach, J. *Chirality* **2009**, *21*, E116−E152. (b) Crawford, T. D. *Theor. Chem. Acc.* **2006**, *115*, 227−245. (c) Rizzo, A.; Coriani, S.; Ruud, K. In *Computational Strategies for Spectroscopy: From Small Molecules to Nano Systems*; Barone, V., Ed.; John Wiley & Sons: Hoboken, NJ, 2012; Chapter 2, pp 77−135. (d) Warnke, I.; Furche, F. *WIREs Comput. Mol. Sci.* **2011**, *2*, 1−17.
(21) (a) Crawford, T. D.; Stephens, P. J. *J. Phys. Chem. A* **2008**, *112*, 1339−1345. (b) Stephens, P. J.; McCann, D. M.; Cheeseman, J. R.; Frisch, M. J. *Chirality* **2005**, *17*, S52−S64. (c) McCann, D. M.; Stephens, P. J. *J. Org. Chem.* **2006**, *71*, 6074−6098.
(22) (a) Ruud, K.; Zanasi, R. *Angew. Chem., Int. Ed.* **2005**, *44*, 3594−3596. (b) Egidi, F.; Barone, V.; Bloino, J.; Cappelli, C. *J. Chem. Theory Comput.* **2012**, *8*, 585−597. (c) Lin, N.; Luo, Y.; Santoro, F.; Zhao, X.; Rizzo, A. *Chem. Phys. Lett.* **2008**, *46*, 144−149.
(23) (a) Mennucci, B.; Cappelli, C.; Cammi, R.; Tomasi, J. *Chirality* **2011**, *23*, 717−729. (b) Mukhopadhyay, P.; Zuber, G.; Wipf, P.; Beratan, D. N. *Angew. Chem., Int. Ed.* **2007**, *46*, 6450−6452. (c) Mukhopadhyay, P.; Zuber, G.; Goldsmith, M.-R.; Wipf, P.; Beratan, D. N. *ChemPhysChem* **2006**, *7*, 2483−2486. (d) Lipparini, F.; Egidi, F.; Cappelli, C.; Barone, V. *J. Chem. Theory Comput.* **2013**, *9*, 1880−1884.
(24) (a) Polavarapu, P. L. *Chirality* **2006**, *18*, 348−356. (b) Polavarapu, P. L. *Chirality* **2008**, *20*, 664−672. (c) Polavarapu, P. L. *Chirality* **2012**, *24*, 909−920.
(25) Han, B.; Li, J.-L.; Ma, C.; Zhang, S.-J.; Chen, Y.-C. *Angew. Chem., Int. Ed.* **2008**, *47*, 9971−9974.
(26) Seebach, D.; Sun, X.; Ebert, M. O.; Schweizer, B.; Purkayastha, N.; Beck, A. K.; Duschmalé, J.; Wennemers, H.; Mukayama, T.; Benohoud, M.; Hayashi, Y.; Reiher, M. *Helv. Chim. Acta* **2013**, *96*, 799−852.
(27) Sahoo, G.; Rahaman, H.; Madarász, A.; Pápai, I.; Melarto, M.; Valkonen, A.; Pihko, P. M. *Angew. Chem., Int. Ed.* **2012**, *51*, 13144−13148.
(28) Ess, D. H.; Jones, G. O.; Houk, K. N. *Adv. Synth. Catal.* **2006**, *348*, 2337−2361.